JAAS

ROYAL SOCIETY OF CHEMISTRY

PAPER

View Article Online
View Journal | View Issue

Cite this: *J. Anal. At. Spectrom.*, 2022, **37**, 2351

High-precision EPMA measurement of trace elements in ilmenite and reference material development†

Li-Hui Jia, *[a] Qian Mao,[a] Heng-Ci Tian,[a] Li-Xing Li,[b] Liang Qi,[c] Shi-Tou Wu,[a] Jiang-Yan Yuan,[a] Liang-Liang Huang[a] and Yi Chen *[ad]

Ilmenite occurs as a common accessory mineral in igneous and metamorphic rocks and is a major constituent in lunar basaltic rocks. The distributions and concentrations of major and trace elements in ilmenite have potential to record temporal changes in melt chemistry and crystal fractionation processes. However, such data are scarce because of the limitations of *in situ* microanalytical technology, the lack of reference materials for trace elements, and the difficulties in analyzing the small needle-like shape of ilmenite. In this study, a natural ilmenite sample derived from the Panzhihua Fe–Ti–V oxide ore deposit was characterized for its major and trace elements in relation to the potential use as reference material. The homogeneity of the studied ilmenite (PZH12-09) was assessed by electron probe microanalysis (EPMA) and laser ablation inductively coupled plasma-mass spectrometry (LA-ICP-MS). It is homogeneous with relative standard deviation (RSD) values within ±3.76% for major elements (Fe, Ti, Mg, and Mn) and ±12.6% for trace elements (Sc, V, Cr, Co, Ni, Zr, Nb, Hf, and Ta), respectively. The relative deviations for major and trace elements determined by solution-mode ICP-MS and *in situ* microanalysis range from 0.11% to 7.71%, suggesting that the PZH12-09 ilmenite can be used as a reference material for *in situ* microanalysis. Furthermore, we developed a high-precision EPMA method to simultaneously determine the major and trace elements of ilmenite. The disadvantage of high detection limits and poor accuracy in trace element analyses were overcome by optimizing the analytical conditions, including the accelerating voltage (20 kV), beam current (200 nA), use of large Bragg crystals (LPET and LLIF), aggregate intensity counting, peak overlap and secondary standard corrections. The measured concentrations of most trace elements are consistent within 10% relative deviation compared with the reference values. The RSD values were within ±15% at various concentrations of trace elements (except for Ni and Nb), indicating the high accuracy and precision characteristics of the EPMA methodology. Detection limits for the trace elements vary from 11 to 27 μg g^{-1} (3σ). The developed method should provide robust trace element data for both extraterrestrial and terrestrial ilmenite samples at high spatial resolution (1–2 μm).

Received 10th July 2022
Accepted 26th September 2022

DOI: 10.1039/d2ja00238h

rsc.li/jaas

1 Introduction

Ilmenite is a widespread accessory mineral in a variety of igneous and metamorphic rocks,[1–3] and is an important megacryst phase in kimberlites.[4–6] It is also the principal ore mineral of titanium in Fe–Ti oxide ore deposits.[7–9] In addition, ilmenite is the major constituent and always as an early and prolonged liquidus phase in high-Ti lunar basalts.[10–13] Ilmenite incorporates elements that are considered both compatible (Cr, V, and Ni) and incompatible (Mn, Nb, Ta, Zr, and Hf) in silicate minerals.[14,15] Previous studies have used the elemental chemistry of ilmenite to interpret the thermal and physical conditions of magmas,[16–18] mantle sources,[5,19,20] and crystal fractionation processes.[14,21] Moreover, ilmenite has been used as an effective tool for diamond exploration[5,22,23] and geospeedometry for estimating the timing of volcanic activity.[18]

Despite the importance of ilmenite in petrological investigations, there is a lack of a reliable analytical methodology for the discrimination of small chemical variations and detection of low-concentration elements at relatively high spatial resolution (micron level). Laser ablation inductively coupled plasma-mass spectrometry (LA-ICP-MS) is a powerful technique for measurement of the content and distribution of trace elements,

[a]*Institute of Geology and Geophysics, Chinese Academy of Sciences, Beijing 100029, China. E-mail: jialihui@mail.iggcas.ac.cn; chenyi@mail.iggcas.ac.cn*

[b]*Institute of Mineral Resources, Chinese Academy of Geological Sciences, Beijing 100037, China*

[c]*Institute of Geochemistry, Chinese Academy of Sciences, Guiyang 550081, China*

[d]*University of Chinese Academy of Sciences, Beijing 100049, China*

† Electronic supplementary information (ESI) available. See https://doi.org/10.1039/d2ja00238h

but is difficult to apply to small (<10 μm) needle-like ilmenite crystals. Electron probe microanalysis (EPMA) is the most suitable *in situ* microanalysis method for the determination of major and minor element concentrations in minerals due to its high resolution, low-cost, and non-destructive characteristics,[24–27] but high detection limits and a lack of secondary reference materials make EPMA unsuitable for trace element analysis. Although there are a few ilmenite standards (*e.g.*, CRN63E, CRN63H, and CRN63K) for routine use in LA-ICP-MS analyses,[15] the rapid consumption of these materials requires the development of a new ilmenite reference material for *in situ* microanalysis. Furthermore, it is necessary to achieve high precision and low detection limits for EPMA measurement of trace elements in ilmenite, particularly for those concentrations below several tens of parts per million.

In this study, we developed and verified the feasibility of natural ilmenite as a new reference material for *in situ* microanalysis by EPMA, LA-ICP-MS, and solution-mode (SM) ICP-MS. Besides, this paper established a new EPMA methodology to effectively lower detection limits and improve accuracy for trace elements in ilmenite. The method may be applied in ascertaining the composition and origin of ilmenite in planetary interiors for better understanding of the formation and evolution of planetary rocks.

2 Sample information and preparation

The studied ilmenite was derived from the Panzhihua (PZH) layered gabbroic intrusion, Emeishan Large Igneous Province, SW China. The intrusion hosts a significant Fe–Ti–V oxide ore deposit, providing an opportunity to select potential ilmenite reference materials. The ilmenites occur in both massive and disseminated Fe–Ti–V oxide ores in the Panzhihua intrusion.[28,29] Massive ores typically contain >80% titanomagnetite with variable amounts of ilmenite, clinopyroxene, plagioclase, and olivine. The sparse silicate minerals are surrounded by oxides. Disseminated ores are generally coarse-grained and consist of ~50 titanomagnetite, ~20% clinopyroxene, ~20% plagioclase, ~10% ilmenite, and minor olivine.[28,29] The size of single ilmenite crystals vary from 0.5 to 5.0 mm, and occur as euhedral–subhedral granular texture with black-gray color.

The PZH12-09 ilmenite samples were collected from mass ores in lens-sharped bodies in the basal part of the lower zone of the intrusion, which extended continuously for more than 12 km along strike and at least 850 m down dip as revealed by drilling.[28,29] The samples were cut with a diamond-bonded brass saw blade and crushed in a steel jaw crusher that had been cleaned thoroughly with deionized water. Approximately 20 g of ilmenite fragments (0.1–2 mm) were hand-picked under a binocular microscope. For measurements performed in this study, a large number fragments were randomly selected and mounted in epoxy resin for *in situ* microanalysis. The mounts were polished and carbon coated before examination with a scanning electron microscope (SEM) for identification of possible submicroscopic mineral inclusions. Ilmenite fragments chosen for further study were likely to be homogenous and free of inclusions based on optical inspection and SEM analysis, and were tested for elemental homogeneity by EPMA and LA-ICP-MS analysis of core-to-rim profiles through the grains. Bulk technique generally require relatively large amounts of sample (about 0.5–1.0 g), preferably in form of powder (200 mesh). Pure ilmenite fragments (~10 g) were therefore pulverized in agate mortars to minimize potential contamination by transition metals in trace element analysis.

3 Analytical techniques

3.1 Energy dispersive spectroscopy (EDS) mapping

EDS mapping was performed using a Zeiss Gemini 450 field-emission scanning electron microscope equipped with an X-ray energy dispersive spectrometer and a pneumatically retractable backscattered electron (BSE) system with a six-segment multimode solid-state BSE detector at Institute of Geology and Geophysics, Chinese Academy of Sciences (IGGCAS), Beijing, China. An acceleration voltage of 15 kV, a beam current of 5 nA, a spot size of 1 μm, and a working distance of 8.5 mm were applied. A maximum resolution of 4096 × 3072 pixels was used to enhance integration point data and step intervals that can increase the mapping accuracy. Single fields of view were stitched for SEM images and EDS mapping results using an automated stage.

3.2 Electron probe microanalysis (EPMA)

Major element concentrations of ilmenite were determined using a JEOL JXA 8100 EPMA at IGGCAS with a 15 kV wavelength dispersive signal (WDS), a 20 nA beam current, and a beam size of 1 μm. Count times were 10 s for peak and 5 s for background per element. Natural minerals and synthetic oxides used for calibration purposes included: diopside (Ca, Si, and Mg), albite (Na and Al), rutile (Ti), bustamite (Mn), K-feldspar (K), NiO (Ni), Fe_2O_3 (Fe), and Cr_2O_3 (Cr). The spectral lines adopted for each element were as follows: Na (129.503), Mn (146.445), K (120.157), Mg (107.451), Si (77.329), Fe (134.921), Al (90.517), Ca (108.315), Ti (89.115), Cr (159.574) and Ni (115.453). Detection limits (1σ) were ~0.02 wt% for Mg, Al, Cr, K, Si, Mn, Ca, and Fe; and ~0.03 wt% for Ni and Ti. A program based on the ZAF procedure was used for data correction (CITIZAF).[30] The routine EPMA method was used only to evaluate ilmenite homogeneity. The other set of routine EPMA measurement was added for comparison using Cameca SXFive instrument. Detailed description of the high-precision EPMA measurement for trace elements in ilmenite was provided in Section 4.3.

3.3 Laser ablation inductively coupled plasma-mass spectrometry (LA-ICP-MS)

3.3.1 IGGCAS-SKLLE. Trace elements of the studied ilmenite were determined using an Agilent 7500a quadrupole ICP-MS instrument (Agilent Technologies, USA) coupled with an Analyte G2 193 nm ArF excimer laser ablation system at the State Key Laboratory of Lithospheric Evolution (SKLLE), IGGCAS. The carrier gas, helium, was passed through the ablation cell, and argon was mixed downstream from the ablation cell. Prior to analysis, the pulse/analog (P/A) factor of the detector

was calibrated using a standard tuning solution. The spot size and frequency of the laser were set to 44 μm and 5 Hz, respectively. The laser energy density was ~4.0 J cm^{-2}. The ablation depth of the laser was approximately 20 to 30 μm.[31] All trace element determinations were carried out using time-resolved analysis in the fast, peak jumping mode. The dwell time for different element was consistent as 10 ms, and the sampling period for 1 cycle was 0.40 s. Each spot analysis included ~20 s background and 60 s sample data acquisition. US National Institute of Standards and Technology (NIST) standard reference material (SRM) 610 glass was used for calibration, and ARM-1 and BCR-2G standards were analyzed for data quality control. Iron (^{57}Fe) was used as an internal standard for concentration calculations. The standards were analyzed twice each, at the beginning and end of data collection (after ten ablations) for unknown samples. Data processing employed the GLITTER program.[32] For most trace elements (>0.10 μg g^{-1}), the accuracy was better than ±10% with analytical precision (1 relative standard deviation, RSD) of ±10%. More details of the analytical procedures are provided by Xie *et al.*[33]

3.3.2 IGGCAS-FIL. *in situ* analysis of trace element compositions of ilmenite was also conducted by LA-ICP-MS method at Fluid Inclusion Laboratory (FIL), IGGCAS. A Coherent Geolas HD 193 nm laser-ablation system was used in conjunction with an Agilent 7900 ICP-MS instrument (Agilent Technologies, USA). Spot diameter was 44 μm, with a laser pulse rate of 6 Hz and energy density of 6 J cm^{-2}. Helium and argon were used as the carrier gas and make-up gas, respectively. The dwell time for each element was 10 ms, with 0.40 s sampling per cycle. Each analysis involved ~20 s of background acquisition (gas blank) and 40 s sample data acquisition. NIST SRM 610 was used as an external calibration standard, and ARM-1 and BCR-2G were analyzed for data quality control. The resulting data were processed based on the GLITTER program.

3.4 Solution-mode inductively coupled plasma-mass spectrometry (ICP-MS)

Three bulk rock samples were coarsely crushed and then powdered to 200 mesh in an agate mortar. Major and selected trace elements were determined using a Jena Plasma Quant MS ICP-MS at Institute of Geochemistry (IG), Chinese Academy of Sciences, Guiyang, using the method of Qi *et al.*[34] About 0.05 g of powdered sample were placed in a PTFE bomb, and 1 ml of HF and 1 ml of HNO_3 were added. The sealed bombs were then placed in an electric oven and heated to 185 °C for about 24 h. After cooling, the bombs were heated on a hot plate to evaporate

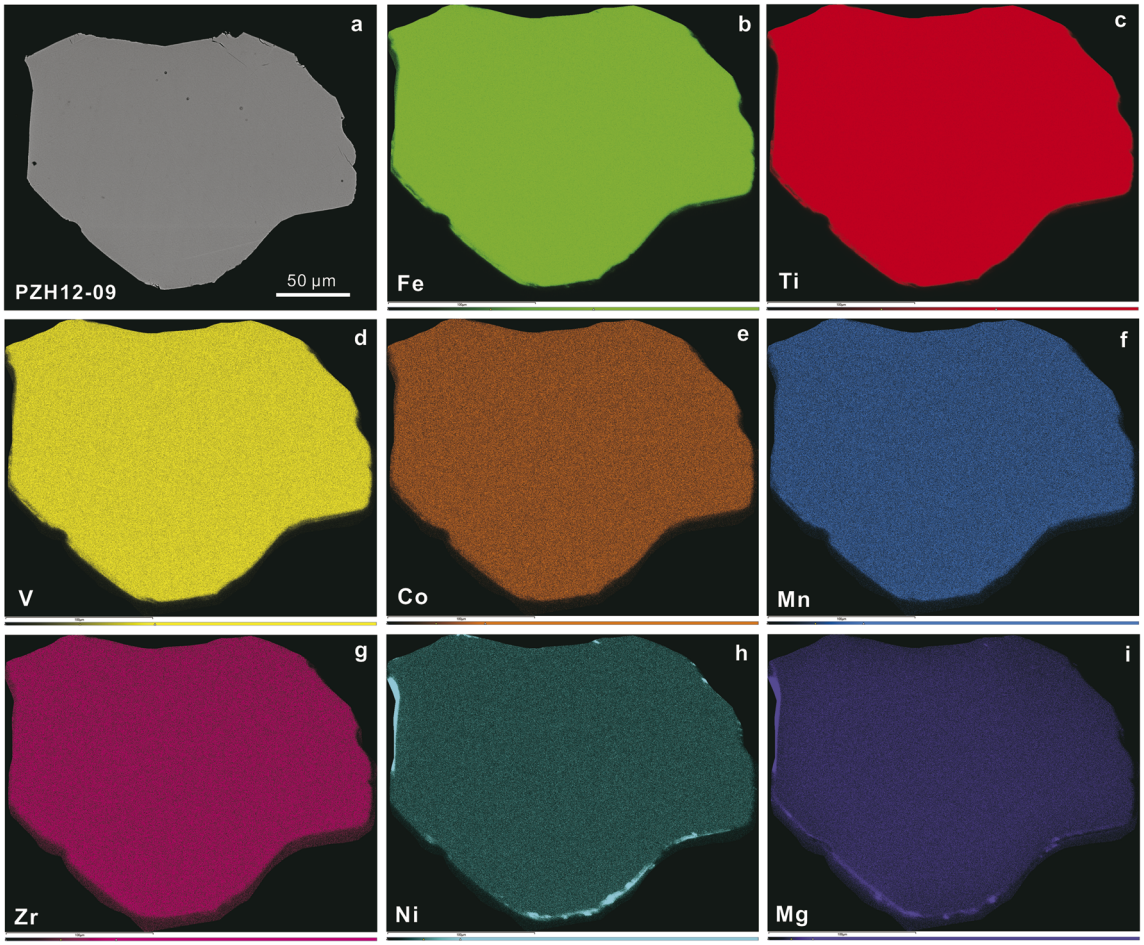

Fig. 1 Representative BSE and EDS mapping images of the PZH12-09 ilmenite sample from the Panzhihua Fe–Ti–V oxide ore deposit.

to dryness. Rh was added (2×10^{-7} g) as an internal standard, together with 2 ml of HNO_3, 1 ml of H_2O_2 (Ti precipitation can be dissolved by H_2O_2) and 3 ml of water were added. The bomb was again sealed and placed in an electric oven at 145 °C for about 3 hours to dissolve the residue. After cooling, the final dilute factor is about 3000 for ICP-MS measurement. Analytical results and uncertainties for reference materials AMH-1 (andesite) and OU-6 (slate) were consistent with the information values.[35,36] Accuracy of the ICP-MS analyses was estimated to be better than ±5–10% for most elements. Results for major and trace elements are reported in Table 3.

4 Results and discussion

4.1 Homogeneity evaluation

A critical requirement for reliable quantitative analyses is the existence of well accepted reference materials of known concentration and matrix, and homogeneous evaluation of elemental distribution is of primary importance.[27,37,38] High-contrast BSE images indicate that the studied ilmenite is likely to be homogeneous with no obvious zonation (Fig. 1a). EDS can provide the elemental distribution in samples on micron to centimeter scales, which is especially important for heterogeneous mineral phases.[39–41] The EDS mapping of the studied ilmenite sample showed no clear compositional variations in Fe, Ti, V, Co, Mn, Zr, Ni, and Mg within individual crystal (Fig. 1b–i). Major and trace elements concentrations of the ilmenite at the μm to mm scale were further evaluated using EPMA and LA-ICP-MS.

The homogeneity of major element contents within and between grains of ilmenite was assessed on 50 pieces of randomly selected fragments, with four spots from core to rim in each fragment being analyzed by JXA 8100 EPMA (ESI Table S1†). Here, the relative standard deviation (RSD) in percent was used as a measure of chemical variation. The PZH12-09 ilmenite has consistent concentrations of major elements (FeO and TiO_2) ranging from 37.2 to 39.0 wt% and from 52.4 to 54.7 wt%, with RSD values of 1.11% and 0.83%, respectively. Except for FeO and TiO_2, only MgO and MnO concentrations were significantly above than detection limits for the routine EPMA method, yielding 6.52–7.21 wt% and 0.46–0.57 wt%, with RSD values of 2.37% and 3.76%, respectively (Table 1 and Fig. 2a). Overall, RSD variations for the PZH12-09 ilmenite were below ±4%, clearly demonstrating that the studied ilmenite is homogeneous with respect to FeO, TiO_2, MgO and MnO. Concentrations of other trace elements were below the detection limits. Furthermore, the representative major elements (Ti and Mn) have normal compositional distributions (Fig. 2b and c), further indicating the homogeneity of the studied ilmenite.

Many trace elements in ilmenite have mass fractions near or below EPMA detection limits, requiring analysis by LA-ICP-MS. Thirty ilmenite fragments from sample PZH12-09 were randomly selected from those previously analyzed by EPMA. Three spots were analyzed in each fragment along the direction of the EPMA profile from core to rim. Results are summarized in ESI Table S2.† The RSD values for Mg, Sc, Mn, Co, Zr, Nb, and Ta were below 10%, while those for V, Cr, and Ni were 10.1–12.5%

Table 1 Comparison of major element (wt%) mass fractions of the PZH12-09 ilmenite determined using routine EPMA, LA-ICP-MS, and SM ICP-MS[a]

Method	Routine EPMA					
Lab	IGGCAS-JXA 8100			IGGCAS-Cameca SXFive		
	Mean	SD	RSD	Mean	SD	RSD
Comment	($n = 200$)			($n = 30$)		
MnO	0.50	0.02	3.76	0.51	0.01	2.66
MgO	6.88	0.16	2.37	6.89	0.19	2.77
FeO	38.2	0.42	1.11	38.4	0.50	1.30
TiO_2	53.7	0.45	0.83	53.4	0.38	0.72
Method	LA-ICP-MS					
Lab	IGGCAS-SKLLE			IGGCAS-FIL		
	Mean	SD	RSD	Mean	SD	RSD
Comment	($n = 45$)			($n = 45$)		
MnO	0.48	0.02	5.10	0.46	0.02	4.41
MgO	6.82	0.25	3.64	6.63	0.30	4.49
FeO						
TiO_2	54.4	1.09	2.01	54.1	1.78	3.28
Method	Solution-mode ICP-MS					
Lab	IGCAS					
	Mean		SD		RSD	
Comment	($n = 3$)					
MnO	0.54		0.01		1.00	
MgO	6.78		0.04		0.57	
FeO	37.4		0.31		0.84	
TiO_2	49.9		0.29		0.58	

[a] SD, standard deviation; RSD, relative standard deviation.

(Table 2). The statistical parameter of the Shapiro–Wilk test[42] indicated the normal distributions for V, Co, Zr, Nb, Ta, and Hf, and the quasi-normal distributions for Sc, Cr, and Ni, likely due to their low mass fractions (ESI Fig. S1†). The H index, an expression of the ratio of the RSD of the analytical data set to the precision of instrumental counting statistics, was proposed to evaluate the compositional homogeneity as described by Harries.[43] An index value of 1 implies that the sample is homogeneous within the analytical uncertainty of individual measurement, while a value of >3 indicates significant chemical heterogeneity.[25,26,44,45] Here, most elements of the PZH12-09 ilmenite plotted near the 1 : 1 line (Fig. 3), suggesting their homogeneity. Although some elements (*e.g.*, Co and Sc) plotted slightly off this line, all RSD values were less than three times their respective analytical repeatability of the instrument. These results indicate negligible heterogeneity of trace elements in the studied ilmenite.

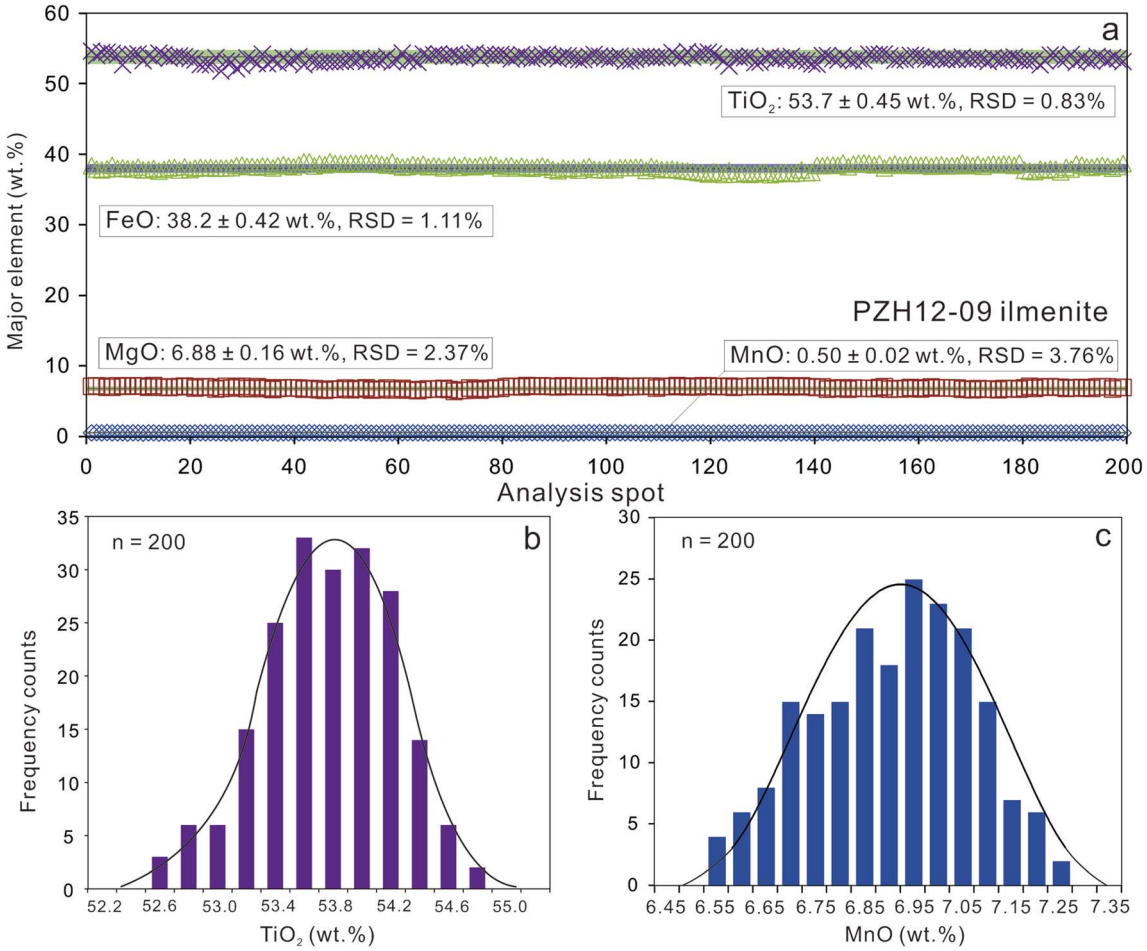

Fig. 2 (a) Variations in major elements (Fe, Ti, Mg, and Mn) of the PZH12-09 ilmenite and (b and c) frequency distributions of EPMA results, indicating the homogeneity of the studied ilmenite. Each point represents one analysis along the core-to-rim line within different grains. Solid lines and shaded areas represent the mean value and 2SD obtained by routine EPMA, respectively. RSD, relative standard deviation.

In summary, data obtained by *in situ* microanalytical techniques indicate that the PZH12-09 ilmenite is homogeneous with respect to major and trace elements at the micron–millimeter scale, and that it is suitable for use as a reference material for instrument calibration and validation of methods.

Table 2 Trace element mass fractions (μg g^{-1}) results for the PZH12-09 ilmenite determined using LA-ICP-MS, SM ICP-MS, and routine EPMA[a]

Method	LA-ICP-MS						Solution-mode ICP-MS			Routine EPMA	
Lab	IGGCAS-SKLLE			IGGCAS-FIL			IGCAS				
	Mean	SD	RSD	Mean	SD	RSD	Mean	SD	RSD		
Comment	($n = 45$)			($n = 45$)			($n = 3$)			IGGCAS-JXA 8100	IGGCAS-Cameca SXFive
Sc	35.6	2.56	7.17	33.4	1.98	5.93	34.5	0.45	1.31	D.L.	D.L.
V	242	19.6	8.07	220	21.0	9.58	237	6.66	2.81	D.L.	D.L.
Cr	21.2	2.05	9.64	20.2	2.17	10.8	22.4	4.92	21.9	D.L.	D.L.
Co	101	6.49	6.44	97.9	4.41	4.50	95.1	4.60	4.84	D.L.	D.L.
Ni	26.1	3.03	11.6	27.7	3.50	12.6	27.4	2.21	8.05	D.L.	D.L.
Zr	83.9	4.66	5.56	81.0	3.76	4.64	84.0	1.61	1.92	D.L.	D.L.
Nb	30.9	1.76	5.68	30.4	1.13	3.71	29.9	0.72	2.41	D.L.	D.L.
Hf	2.21	0.19	8.46	2.20	0.11	4.97	2.15	0.18	8.18	D.L.	D.L.
Ta	2.89	0.22	7.60	2.79	0.19	6.97	2.73	0.07	2.44	D.L.	D.L.

[a] D.L., below detection limits; RD, standard deviation; RSD, relative standard deviation.

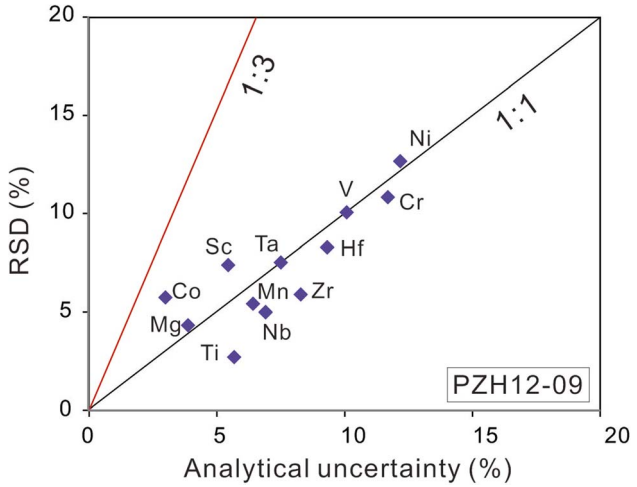

Fig. 3 Assessment of homogeneity of trace elements in the PZH12-09 ilmenite obtained using LA-ICP-MS. Homogeneity index value of 1 and 3 (red line) is shown. All trace elements plot below the 1 : 3 line, indicating their homogeneity.

4.2 Preliminary values and uncertainties

Reference values are reported only for data obtained from at least three laboratories that are in statistical agreement, based on independent and well-defined measurement techniques.[46,47] All the investigated major elements (Fe, Ti, Mg, and Mn) analyzed by routine EPMA and SM ICP-MS in present study plot well along the 1 : 1 correspondence line (Fig. 4a). A comparison of LA-ICP-MS and SM ICP-MS results also indicated consistency for most of elements investigated (Fig. 4b and ESI Table S3†), with Mg, Sc, V, Ni, Zr, Nb, Hf, and Ta having relative deviations within ±5% (Table 1). Aluminum data obtained by SM ICP-MS are higher than those by LA-ICP-MS, possibly related to the rare fine plagioclase inclusions in ilmenite samples. Therefore, Na, K, Al, Ca, and Si as major elements of plagioclase should be removed from results for the PZH12-09 ilmenite to ensure the validity of the ilmenite reference material. However, results obtained by the different measurement techniques are generally consistent (Fig. 4).

The determination of reference values and their uncertainties of the studied ilmenite at the 95% confidence level closely followed ISO guidelines (ISO 17034 Guide 35 2017).[48] To obtain reference values for the PZH12-09 ilmenite, arithmetic means of data from all contributing laboratories were used as the best estimates of true values.[46] Outliers were rejected if the data were unacceptable for technical reasons, such as measurements near the detection limits or calibration errors.[37,49] The uncertainty, U, of the reference value at a 95% confidence level is given by

$$U = k \times u \quad (1)$$

where k represents the Student's t distribution, with a value of 3 for $n < 7$;[37,49] and "u" is based mainly on three components: the standard deviation of the mean (Y_{mean} of n contributing laboratory mean data), the VAR_{inhomo} (inhomogeneity of ilmenite), and VAR_{bias} for between-laboratory biases,[46] which were combined as follows:

$$u^2 = VAR(Y_{mean}/\sqrt{n}) + VAR_{imhomo} + VAR_{bias} \quad (2)$$

The *in situ* microanalysis results suggested that the PZH12-09 ilmenite is homogeneous, so the second term was very small and thus ignored. Furthermore, results obtained by different techniques were generally consistent, so any between-laboratory bias was insignificant and affected little.

Reference values and their overall uncertainties are listed in Table 3. The n refers to the number of independent measurements contributing to the reference value, 2 s refers to two times standard deviation, 2SE refers to times standard error (2 s divided by $\sqrt{n}$), and U refers to the overall expanded uncertainty at the 95% confidence level.

4.3 High-precision EPMA measurement for trace elements in ilmenite

Based on the morphological characteristics of natural ilmenite and the development of *in situ* microanalysis, EPMA with high spatial resolution is an excellent choice for analysis of major and trace elements in ilmenite samples.[11,27,37,49,50] A voltage of 15

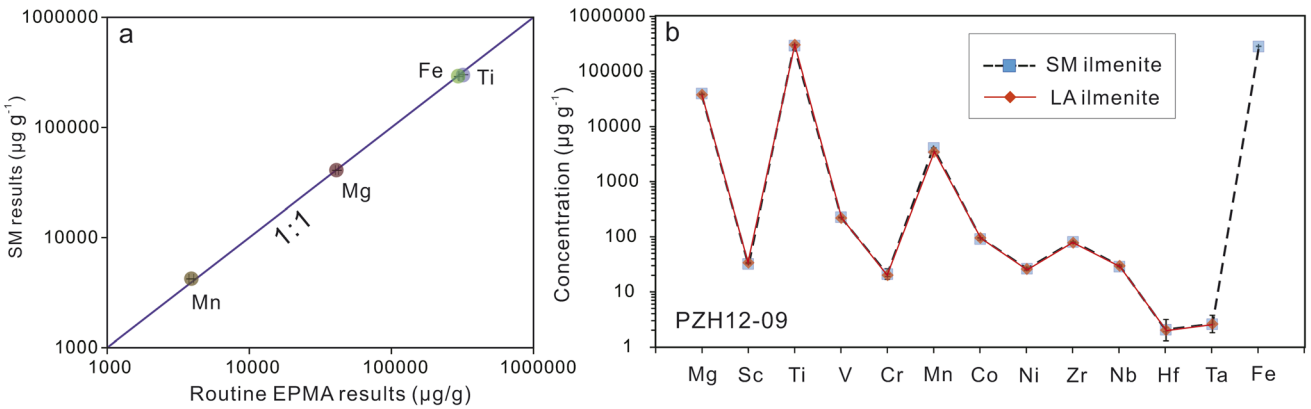

Fig. 4 (a) Comparison of major elements of the PZH12-09 ilmenite determined by routine EPMA and SM ICP-MS. The 1 : 1 line is shown for comparison. (b) Major and trace elements contents obtained by LA-ICP-MS and SM ICP-MS for the ilmenite sample, indicating that the PZH12-09 ilmenite is suitable for use as a reference material for ilmenite *in situ* microanalysis.

Table 3 Preliminary reference values for major (wt%) and trace elements (μg g^{-1}) of the PZH12-09 ilmenite

	In situ microanalysis				Bulk technique						
Method	EPMA		LA-ICP-MS		Solution-mode ICP-MS		Preliminary information value				
Comment	Mean	1 SD	Mean	1 SD	Mean	1 SD	Value	*n*	2 SD	2 SE	*U*
MnO	0.50	0.02	0.47	0.03	0.54	0.01	0.51	5	0.03	0.01	0.02
MgO	6.88	0.17	6.72	0.29	6.78	0.04	6.79	5	0.33	0.15	0.22
FeO	38.2	0.44			37.4	0.31	37.8	3	0.75	0.43	0.65
TiO_2	53.6	0.44	54.3	1.47	49.9	0.29	52.6	5	1.47	0.66	0.99
Sc			34.5	2.55	34.5	0.45	34.5	3	3.00	1.73	2.59
V			231	23.2	237	6.66	234	3	29.9	17.2	25.9
Cr			20.7	2.16	22.4	4.92	21.6	3	7.08	4.09	6.13
Co			99.3	5.68	95.1	4.60	97.2	3	10.3	5.94	8.91
Ni			26.9	3.36	27.4	2.21	27.1	3	5.56	3.21	4.82
Zr			82.5	4.46	84.0	1.61	83.2	3	6.07	3.50	5.25
Nb			30.7	1.49	29.9	0.72	30.3	3	2.21	1.28	1.91
Hf			2.20	0.15	2.15	0.18	2.18	3	0.33	0.19	0.28
Ta			2.84	0.21	2.73	0.07	2.79	3	0.28	0.16	0.24

Table 4 Analytical conditions of high-precision EPMA measurement for trace elements in ilmenite

Element	Spectrometer	Linear	Calibration standard	Analysis crystal	Acceleration voltage (kV)	Beam current (nA)	Peak position	$B_g -$ (Sin $\theta \times 10^5$)	$B_g +$ (Sin $\theta \times 10^5$)	Slope	Peak counting time (s)	Background counting time (s)
Mg	Sp1	Kα	Pure MgO	TAP	20	200	38 504	−1500	950		20	10
Sc	Sp4	Kα	Pure ScO	LPET	20	200	34 651	−500	350		80	40
Zr	Sp4	Lα	Baddeleyite	LPET	20	200	69 379	−700	500		120	60
Nb	Sp4	Lα	Pure Nb_2O_5	LPET	20	200	65 421	−500	350		120	60
Ti	Sp2	Kα	$SrTiO_3$	LLIF	20	200	68 254	−1000	1000		10	5
Fe	Sp3	Kα	Kaersutite	LLIF	20	200	48 090	−1000	1000		10	5
Mn	Sp2	Kα	Pure MnO	LLIF	20	200	52 196	−1000	1000		30	15
Co	Sp3	Kα	Pure CoO	LLIF	20	200	44 429		500	1	120	120
Cr	Sp2	Kα	Pure Cr_2O_3	2 LLIF	20	200	56 861	−350	350		120	60
Ni	Sp3	Kα	Pure NiO	LLIF	20	200	41 169	−700	700		120	60
V	Sp2	Kα	Pure V	LLIF	20	200	62 169	−800		1	120	120

kV and beam current of 20 nA are generally used for routine EPMA analysis for ilmenites in most laboratories, with detection limits of hundreds of μg g^{-1} and accuracies as low as 50% for trace elements. To achieve lower detection limits and higher accuracy, the following effective approaches were applied on a Cameca SXFive EPMA instrument at the IGGCAS.

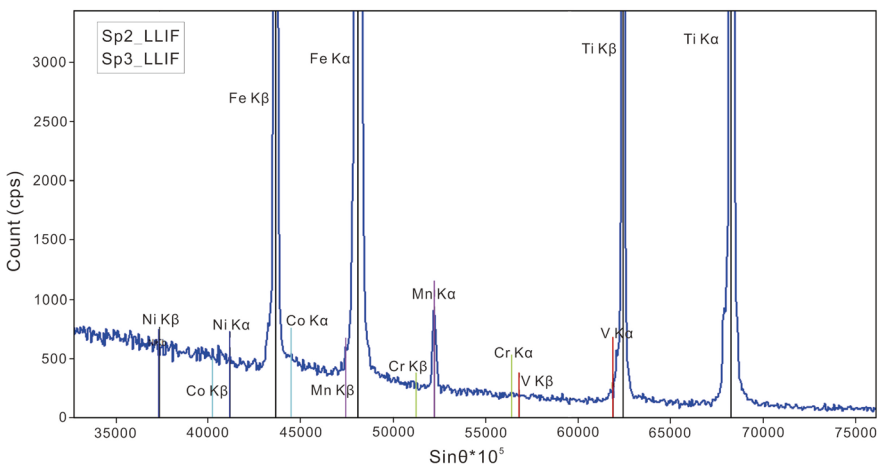

Fig. 5 Wavelength dispersive scans with two LLIF analyzing crystals in a Cameca SXFive EPMA instrument, showing spectral interferences of Ti (Kβ) to V (Kα), Fe (Kβ) to Co (Kα), Cr (Kβ) to Mn (Kα), and V (Kβ) to Cr (Kα).

There are several general approaches for improving the precision of EPMA trace elements analysis including increasing accelerating voltage, beam current, or count integration time.[24,27,51] Higher accelerating voltage and beam current increase the ionization efficiency and electron flux, and increased counting time improves statistics for greater precision by increasing the total numbers of photons integrated.[52,53] Additionally, some engineered strategies are also implemented to lower detection limits, such as using larger Bragg analysis crystals to improve the geometric efficiency of the instrument, and using aggregate intensity counting software to improve counting statistics.[24,26,54] After detailed comparisons of Cameca SXFive EPMA conditions, the following approaches were set in this study: (1) a higher acceleration voltage of 20 kV was used to balance precision and spatial resolution (1–2 μm); (2) a higher beam current of 200 nA and longer peak counting time (20–120 s) were applied for trace elements to achieve a detection limit of around 10 μg g^{-1} (3σ); (3) three large (2 LLIF and 1 LPET) Bragg crystals and one normal (TAP) crystal were used for higher sensitivity and counting rates; (4) the software capacity of aggregate intensity counting was used, such as LLIF crystals in spectrometer 2 and 3 for Cr. Detailed settings are provided in Table 4.

Table 5 Major and trace element composition (μg g^{-1}) of the PZH12-09 ilmenite using high-precision EPMA method[a]

Comment	Mg	Sc	Zr	Nb	Ti	Fe	Mn	Co	Cr	Ni	V
D.L. (3σ)	18	11	20	22	70	61	27	21	13	17	19
PZH12-09-1	42 965	35.6	83.5	25.6	316 710	306 643	3938	109.0	19.7	34.6	223
PZH12-09-2	43 348	34.0	79.8	18.0	316 939	307 901	4007	108.5	18.9	26.9	215
PZH12-09-3	43 015	39.9	71.4	12.0	317 807	307 730	4015	92.3	23.7	18.4	221
PZH12-09-4	43 363	33.0	77.0	31.6	317 518	306 622	3985	112.1	22.3	39.5	180
PZH12-09-5	39 904	40.6	76.7	44.5	316 653	307 435	3961	99.9	21.1	20.8	220
PZH12-09-6	40 198	41.5	66.1	31.3	317 065	307 064	3922	110.8	25.1	20.2	211
PZH12-09-7	40 159	38.4	67.2	34.8	317 936	307 921	3970	98.3	21.4	34.9	241
PZH12-09-8	40 210	41.2	84.2	31.4	318 067	306 321	3916	113.7	25.0	29.1	256
PZH12-09-9	40 336	44.1	83.5	38.3	316 464	306 172	4008	112.0	18.9	22.3	200
PZH12-09-10	40 620	41.7	84.5	29.0	316 127	307 429	4032	99.8	20.6	22.0	244
PZH12-09-11	40 199	40.1	79.1	28.0	315 979	307 175	4027	112.0	23.1	23.1	208
PZH12-09-12	40 110	40.2	67.0	33.0	313 261	306 585	4000	93.5	21.0	23.1	207
PZH12-09-13	39 830	38.2	82.6	24.0	315 486	304 516	4062	85.5	24.3	16.1	209
PZH12-09-14	39 940	32.2	81.4	22.1	319 259	303 620	4090	112.0	23.9	26.0	206
PZH12-09-15	43 270	34.9	77.7	18.1	316 155	303 242	4074	94.0	20.2	16.5	251
PZH12-09-16	43 206	38.2	72.9	18.1	316 239	304 868	4062	85.0	28.2	18.0	223
PZH12-09-17	43 309	37.2	81.0	36.8	311 175	305 784	3981	90.4	24.4	15.1	215
PZH12-09-18	42 965	35.2	93.0	18.0	315 072	306 555	4021	90.0	22.3	19.8	221
PZH12-09-19	43 231	35.9	67.0	27.0	314 253	304 898	3938	94.0	25.8	23.5	220
PZH12-09-20	43 298	32.6	88.9	28.8	313 637	304 688	4015	102.0	21.0	35.0	211
PZH12-09-21	43 015	33.4	76.2	27.5	320 672	310 886	3985	92.0	25.0	27.0	240
PZH12-09-22	39 904	35.6	81.0	32.8	318 136	309 384	3961	65.0	19.0	18.0	251
PZH12-09-23	40 198	30.1	81.4	20.1	317 390	312 913	3938	100.0	31.0	29.0	200
PZH12-09-24	40 159	36.0	76.4	33.6	316 181	312 435	4007	107.0	33.0	21.0	244
PZH12-09-25	40 210	34.0	80.0	26.3	317 460	311 991	3916	84.0	31.0	20.0	208
PZH12-09-26	40 336	40.0	71.0	26.1	315 509	308 856	4008	89.0	25.0	25.0	207
PZH12-09-27	40 620	33.0	95.0	25.5	317 893	311 325	4032	87.0	20.0	29.0	209
PZH12-09-28	40 199	36.0	85.0	37.0	317 064	313 495	4027	89.0	21.0	22.0	206
PZH12-09-29	40 110	42.0	79.0	30.4	318 568	313 379	4000	109.0	25.0	22.0	251
PZH12-09-30	39 830	38.0	67.0	41.4	315 851	316 473	4062	109.0	22.0	23.0	199
PZH12-09-31	39 940	41.0	78.0	26.0	316 710	306 643	4090	92.0	20.0	23.0	179
PZH12-09-32	43 235	40.0	73.0	18.0	316 939	307 901	4074	112.0	28.0	26.0	196
PZH12-09-33	42 859	42.0	78.0	37.0	317 807	307 730	4062	100.0	24.0	21.0	242
PZH12-09-34	42 715	32.0	89.0	32.0	317 518	306 622	3981	111.0	22.0	26.0	231
PZH12-09-35	43 155	35.0	76.0	45.0	316 653	307 435	4020	98.0	26.0	16.0	244
PZH12-09-36	42 363	38.0	75.0	30.0	317 065	307 064	3955	114.0	23.0	20.0	238
PZH12-09-37	42 948	35.0	81.0	15.0	317 936	307 921	3959	114.0	23.0	17.0	245
PZH12-09-38	42 771	36.0	76.0	23.0	318 067	306 321	3953	115.0	22.0	24.0	262
PZH12-09-39	42 981	33.0	71.0	31.0	316 464	306 172	3956	100.0	21.0	18.0	239
PZH12-09-40	43 014	33.0	76.0	26.0	316 127	307 429	3922	90.0	24.0	26.0	234
Mean	41 601	36.9	78.2	28.4	316 695	307 889	3998	99.8	23.4	23.4	223
1 SD	1487	3.49	6.92	7.8	1660	2906	50.1	11.4	3.34	5.67	20.8
RSD	3.58	9.46	8.84	27.5	0.52	0.94	1.25	11.4	14.3	24.2	9.36
Information value	40 765	34.5	83.2	30.3	315 225	293 924	3930	97.2	21.6	27.1	234
Relative deviation (%)	−2.05	−7.13	6.00	6.42	−0.47	−4.75	−1.73	−2.66	−8.48	13.61	4.78

[a] SD, standard deviation; RSD, relative standard deviation.

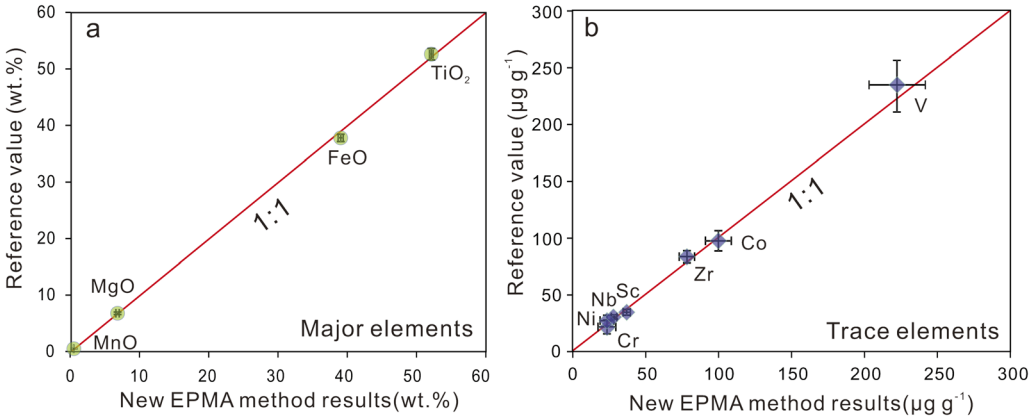

Fig. 6 Comparison of major and trace element mass fractions obtained using high-precision EPMA with results from (a) SM ICP-MS and (b) LA-ICP-MS. The 1 : 1 lines are provided for comparison. Each point represents the mean value of 40 spots, and the bars shown for spot represent two times standard deviation.

Although precision and detection limits can be improved by these methods, accuracy often remains a limiting factor for EPMA trace element measurements. The primary cause for most accuracy errors is the result of spectral interference of different elements and/or the determination of background intensity.[24,55,56] To avoid these situations, we undertook high-sensitivity wavelength scans on each side of the peak for Sc, Zr, Nb, Ti, Fe, Mn, Co, Cr, V, and Ni using the ilmenite standard to identify peak positions and optimal background positions. There are two main types of spectral interference for trace elements in ilmenite: (1) spectral interferences from secondary emission lines of major elements in the sample matrix, such as peak overlaps of Ti (Kβ) to V (Kα) and Fe (Kβ) to Co (Kα); and (2) spectral interference by secondary lines from other trace elements, such as peak overlaps of Cr (Kβ) to Mn (Kα) and V (Kβ) to Cr (Kα) (Fig. 5). Initially, V (Kβ) was used to ignore the intensive spectral interference of Ti (Kβ) to V (Kα). However, the counting intensity of V (Kβ) was not only too weak to identify, but also easily interfered by Cr (Kα) (Fig. 5). Therefore, unilateral background intensity selection was applied to obtain more accurate background intensities for V (Kα) and Co (Kα), with the slopes set to 1 (Table 2). In addition, the spectral interferences of peak positions, such as Cr (Kβ) to Mn (Kα) or V (Kβ) to Cr (Kα), were also corrected by deducting the false peak counting intensity of other elements in pure metal or oxide standards. To monitor and correct these inaccuracies, a quantitative secondary standard correction for EPMA was implemented with our new PZH12-09 ilmenite standard being incorporated into the traditional ZAF correction.

The PZH12-09 ilmenite standard was further analyzed to test the accuracy and precision of the EPMA methodology in this study. Results for most elements were consistent with the reference values within ±10% (2SD, Tables 5, S4† and Fig. 6), except for Ni (13.6%), which may be resulted by its low concentration (23 μg g^{-1}). Thus, the optimal EPMA method has high analytical accuracy. In addition, the analytical precision (reproducibility) established by 40 spots on the PZH12-09 ilmenite varied from 0.52% to 14.3% at various concentrations of trace elements, except for the low abundances (<30 μg g^{-1}) Ni and Nb (~20%). Detection limits are 18 μg g^{-1} for Mg, 11 μg g^{-1} for Sc, 20 μg g^{-1} for Zr, 22 μg g^{-1} for Nb, 27 μg g^{-1} for Mn, and 21 μg g^{-1} for Co, 13 μg g^{-1} for Cr, 17 μg g^{-1} for Ni, and 19 μg g^{-1} for V, based on a 3σ estimate of the measured background variance (Table 5).

5 Conclusions

A natural ilmenite sample (PZH12-09) sourced from the Panzhihua Fe–Ti–V oxide ore deposit was evaluated using EDS mapping, EPMA, and LA-ICP-MS. Results suggest that it is homogeneous, with RSD values within ±3.76% (1 SD) for major elements (Fe, Ti, Mg, and Mn) and ±12.6% (1 SD) for trace elements (Mg, Sc, Mn, Co, Zr, Nb, Ta, V, Cr, Ni, and Hf), respectively. The results obtained by solution-mode ICP-MS and *in situ* microanalysis show good agreements for most elements, suggesting that the PZH12-09 sample is suitable for use as a reference material for ilmenite *in situ* microanalysis. Based on the new ilmenite standard, a high-precision EPMA method was developed for trace elements at the <100 ppm level in ilmenite using a high accelerating voltage of 20 kV and beam current of 200 nA, together with a combination of approaches involving large Bragg crystals, long count integration time, aggregate intensity counting function, enhancement of peak/background ratios, suppression of peak spectral interferences, and secondary standard corrections. These approaches resulted in excellent precision and accuracy at levels well below 100 ppm with high spatial resolution (1–2 μm) and low detection limits (11–27 μg g^{-1}, 3σ). The reliable methodology presented here is potentially useful in elucidating the chemical and physical history of ilmenite and the related host rocks.

Author contributions

All authors listed contributed to the study conception and design. Conceptualization: Li-Hui Jia and Yi Chen; methodology, Li-Hui Jia; software, Qian Mao; validation, Li-Hui Jia and

Qian Mao; formal analysis, Liang Qi, Shi-Tou Wu, Jiang-Yan Yuan, Liang-Liang Huang, Qian Mao and Li-Hui Jia; investigation, Li-Hui Jia and Li-Xing Li; resources, Heng-Ci Tian and Li-Xing Li; data curation, Qian Mao; writing-original draft preparation, Li-Hui Jia; writing-review & editing, Li-Hui Jia; visualization, Li-Hui Jia; supervision, Yi Chen; project administration, Li-Hui Jia; funding acquisition, Li-Hui Jia and Yi Chen. All authors read and approved the final manuscript.

Conflicts of interest

No potential conflict of interest was reported by the authors.

Acknowledgements

This study was financially supported by the National Natural Science Foundation of China (No. 42002096, 42172064), the Key Research Program of the Chinese Academy of Sciences (ZDBS-SSW-JSC007-15), and the Key Research Program of the Institute of Geology and Geophysics, Chinese Academy of Sciences (IGGCAS-202101).

References

1 B. F. Windley, *J. Geol. Soc.*, 1993, **150**, 39–50.
2 J. Lawford Anderson and J. Morrison, *Lithos*, 2005, **80**, 45–60.
3 R. P. Liferovich and R. H. Mitchell, *Crystallogr. Rep.*, 2006, **51**(3), 383–390.
4 L. Carmody, L. A. Taylor, K. G. Thaisen, *et al.*, Ilmenite as a diamond indicator mineral in the Siberian Craton: a tool to predict diamond potential, *Econ. Geol.*, 2014, **109**(3), 775–783.
5 A. B. Golubkova, A. A. Nosova and Y. O. Larionova, *Geochem. Int.*, 2013, **51**, 353–381.
6 A. V. Kargin, A. A. Nosova, L. V. Sazonova, E. V. Peresetskaya, Y. Y. Golubeva, N. M. Lebedeva, V. V. Tretyachenko, V. A. Khvostikov and J. P. Burmii, *Petrology*, 2020, **28**, 315–337.
7 B. Charlier, J. C. Duchesne and J. Vander Auwera, *Chem. Geol.*, 2006, **234**, 264–290.
8 I. V. Ashchepkov, N. V. Alymova, A. M. Logvinova, N. V. Vladykin, S. S. Kuligin, S. I. Mityukhin, H. Downes, Y. B. Stegnitsky, S. A. Prokopiev, R. F. Salikhov, V. S. Salikhov and O. S. Khmel'nikova, *Solid Earth*, 2014, **5**, 915–938.
9 C. E. Morisset, J. S. Scoates and D. Weis, *Can. Mineral.*, 2010, **48**, 821–849.
10 S. E. Harggerty, *Geochim. Cosmochim. Acta*, 1973, **37**, 857–867.
11 J. J. Papike, J. M. Karner and C. K. Shearer, *Am. Mineral.*, 2005, **90**, 277–290.
12 L. Alexander, J. F. Snape, I. A. Crawford, K. H. Joy and H. Downes, *Meteorit. Planet. Sci.*, 2014, **155**, 1288–1304.
13 L. Tokle and K. M. Robertson, *Eur. J. Mineral.*, 2019, **31**, 473–483.
14 B. Charlier, O. Skar, A. Korneliussen, J. C. Duchesne and J. V. Auwera, *Contrib. Mineral. Petrol.*, 2007, **154**, 119–134.
15 P. H. Donohue, A. Simonetti and C. R. Neal, *Geostand. Geoanal. Res.*, 2012, **36**, 61–73.
16 C. R. Bacon and M. M. Hirschmann, *Am. Mineral.*, 1988, **73**(1–2), 57–61.
17 M. S. Ghiorso and B. W. Evans, *Am. J. Sci.*, 2008, **308**(9), 957–1039.
18 K. B. Prissel, M. J. Krawczynski and J. A. V. Orman, *Contrib. Mineral. Petrol.*, 2020, **175**, 62.
19 J. D. Grigsby, *J. Sediment. Res.*, 1992, **62**, 331–337.
20 J. M. Thompson, K. Goemann, I. Belousov, K. Jenkins, A. Kobussen, W. Powell and L. Danyushevsky, *J. Anal. At. Spectrom.*, 2021, **36**, 1244–1260.
21 E. M. Sakoma and R. F. Martin, *Mineral. Mag.*, 2002, **66**, 591–604.
22 J. J. Gurney and P. Zweistra, *J. Geochem. Explor.*, 1995, **53**, 293–309.
23 C. E. Fipke, J. J. Gurney and R. O. Moore, *Geol. Surv. Can., Bull.*, 1995, **423**, 1–86.
24 J. J. Donovan, H. A. Lowers and B. G. Rusk, *Am. Mineral.*, 2011, **96**, 274–282.
25 M. J. Pankhurst, R. Walshaw and D. Morgan, *Geostand. Geoanal. Res.*, 2017, **41**, 85–91.
26 V. G. Batanova, J. M. Thompson, L. V. Danyushevsky, M. V. Portnyagin, D. Garbe-Schonberg, E. Hauri, J. I. Kimura, Q. Chang, R. Senda, K. Goemann, C. Chauvel, S. Campillo, D. A. Lonov and A. V. Sobolev, *Geostand. Geoanal. Res.*, 2019, **43**, 453–473.
27 L.-H. Jia, Y. Chen, Q. Mao, D. Zhang, J.-Y. Yuan, X.-G. Li, S.-T. Wu and D.-P. Zhang, *At. Spectrosc.*, 2022, **43**, 42–52.
28 K.-N. Pang, M.-F. Zhou, D. Lindsley, D.-G. Zhao and J. Malpas, *J. Petrol.*, 2008, **49**, 295–313.
29 M.-F. Zhou, P. T. Robinson, C. M. Lesher, R. R. Keays, C.-J. Zhang and J. Malpas, *J. Petrol.*, 2005, **46**, 2253–2280.
30 J. T. Armstrong, *Microbeam Anal.*, 1995, **4**(3), 177–200.
31 S.-T. Wu, C.-X. Xu, K. Simon, Y.-L. Xiao and Y.-P. Wang, *Rock Miner. Anal.*, 2017, **36**(5), 451–459 (in Chinese with English abstract).
32 W. Griffin, W. Powell, N. J. Pearson and S. O Reilly, in *Laser Ablation-ICP-MS in the Earth Sciences: Current Practices and Outstanding Issues*, ed. P. Sylvester, 2008, pp. 308–311.
33 L. W. Xie, Y.-B. Zhang, H.-H. Zhang, J.-F. Sun and F.-Y. Wu, *Chin. Sci. Bull.*, 2008, **53**, 1565–1573.
34 L. Qi, J. Hu and D. C. Gregoire, *Talanta*, 2000, **51**, 507–513.
35 P. J. Potts and J. S. Kane, *Geostand. Geoanal. Res.*, 2005, **29**, 233–236.
36 M. Thompson, P. J. Potts, J. S. Kane and S. Wilson, *Geostand. Geoanal. Res.*, 2000, **24**, E1–E28.
37 K. P. Jochum, D. B. Dingwell, A. Rocholl, B. Stoll, A. W. Hofmann, S. Becher, A. Besmehn, D. Bessette, H. J. Dietze, P. Dulski, J. Erzinger, E. Hellebrand, P. Hoppe, I. Hom, K. Janssens, G. A. Jenner, M. Klein, W. F. McDonough, M. Maetz, K. Mezger, C. Munker, I. K. Nikogosian, C. Pickhardt, I. Raczek, D. Rhede, H. M. Seufert, S. G. Simakin, A. V. Sobolev, B. Spattel, S. Straub, L. Vincze, A. Wallianos, G. Wechwerth, S. Weyer, D. Wolf and M. Zimmer, *Geostand. Geoanal. Res.*, 2000, **24**, 87–133.

38 D. Harries, *Chem. Erde*, 2014, **74**, 375–384.
39 R. Cossio, A. Borghi and R. Ruffini, *Microsc. Microanal.*, 2002, **8**(2), 139–149.
40 D. K. Tinkham and E. D. Ghent, *Am. Mineral.*, 2005, **90**, 737–744.
41 P. Lanari, A. Vho, T. Bovay, L. Airaghi, S. Centrella, *Quantitative compositional mapping of mineral phases by electron probe micro-analyser*, Geological Society, London, Special Publications, 2018, p. SP478.4.
42 N. M. Razali and Y. B. Wah, *Geostand. Geoanal. Res.*, 2011, **2**, 21–33.
43 D. Harries, *Chem. Erde*, 2014, **74**, 375–384.
44 F. R. Boyd, L. W. Finger and F. Chayes, *Carnegie Inst. Wash. Year Book*, 1967, **67**, 210–215.
45 P. J. Potts, A. G. Tindle and M. C. Isaacs, *Am. Mineral.*, 1983, 1237–1242.
46 J. S. Kane, P. J. Potts, M. Wiedenbeck, J. Carignan and S. Wilson, *Geostand. Geoanal. Res.*, 2003, **27**, 227–244.
47 J. S. Kane, P. J. Potts, T. Meisel and M. Wiedenbeck, *Geostand. Geoanal. Res.*, 2007, **31**, 285–288.
48 ISO 17034 Guide 35, International Organisation for Standardization, Geneva, 2017, p. 105.
49 K. P. Jochum, K. Stoll, K. Herwig, M. Willbold, A. W. Hofmann, M. Amini, S. Aarburg, W. Abouchami, E. Hellebrand, B. Mocek, I. Raczek, A. Stracke, O. Alard, C. Bouman, S. Becker, M. Dücking, H. Brätz, R. Klemd, D. de Bruin, D. Canil, D. Cornell, C. J. de Hoog, C. Dalpé, L. Danyushevsky, A. Eisenhauer, Y. J. Gao, J. E. Snow, N. Groschoph, D. Günther, C. Latkoczy, M. Guillong, E. H. Hauri, H. E. Höfer, Y. Lahaye, K. Horz, D. E. Jacob, S. A. Kasemann, A. J. R. Kent, T. Ludwig, T. Zack, P. R. D. Mason, A. Meixner, M. Rosner, K. Misawa, B. P. Nash, J. Pfänder, W. R. Premo, W. D. Sun, M. Tiepolo, R. Vannucci, T. Vennemann, D. Wayne and J. D. Woodhead, *Geochem., Geophys., Geosyst.*, 2006, **7**, 1–44.
50 P. Nadoll and A. E. Koenig, *J. Anal. At. Spectrom.*, 2011, **26**, 1872–1877.
51 S. J. B. Reed, *Electron Microprobe Analysis and Scanning Electron Microscopy in Geology*, 2005.
52 J. J. Donovan and M. Rowe, *Geochim. Cosmochim. Acta*, 2005, **69**(1), 10.
53 D. Zhang, Y. Chen, W. Yang, J. H. Fournelle, J.-L. Ji, B. Su, Q. Mao, L.-H. Jia, J.-Y. Yuan and X.-G. Li, *At. Spectrosc.*, 2022, **43**, 28–41.
54 M. J. Jercinovic, M. L. Williams and E. D. Lane, *Chem. Geol.*, 2008, **254**, 197–215.
55 M. J. Jercinovic and M. L. Williams, *Am. Mineral.*, 2005, **90**, 526–546.
56 M. J. Jercinovic, M. L. Williams, J. Allaz and J. J. Donovan, *Microsc. Microanal.*, 2011, **17**, 576–577.